THE JOURNAL OF PHYSICAL CHEMISTRY A



A: Spectroscopy, Molecular Structure, and Quantum Chemistry

# Enhancing the Sensitivity of Solid-State NMR Experiments with Very Low-Gyromagnetic Ratio Nuclei with Fast MAS and Proton Detection

Amrit Venkatesh, Matthew J. Ryan, Abhranil Biswas, Kasuni C. Boteju, Aaron D. Sadow, and Aaron J Rossini

*J. Phys. Chem. A*, **Just Accepted Manuscript** • DOI: 10.1021/acs.jpca.8b05107 • Publication Date (Web): 04 Jun 2018

# Enhancing the Sensitivity of Solid-State NMR Experiments with Very Low-Gyromagnetic Ratio Nuclei with Fast MAS and Proton Detection

*Amrit Venkatesh,[1,2] Matthew J. Ryan,[1] Abhranil Biswas,[1] Kasuni C. Boteju,[1] Aaron D. Sadow,[1,2] Aaron J. Rossini[1,2*]*

[1]*Iowa State University, Department of Chemistry, Ames, IA, USA, 50011*

[2]*US DOE Ames Laboratory, Ames, Iowa, USA, 50011*

AUTHOR INFORMATION

**Corresponding Author**

*e-mail: arossini@iastate.edu, phone: 515-294-8952.

## Abstract

Many transition metals commonly encountered in inorganic materials and organometallic compounds possess NMR-active nuclei with very low gyromagnetic ratios (γ) such as $^{89}$Y, $^{103}$Rh, $^{109}$Ag and $^{183}$W. A low-γ leads to poor NMR sensitivity and other experimental challenges. Consequently, nuclei with low-γ are often impossible to study with conventional solid-state NMR methods. Here, we combine fast magic angle spinning (MAS) and proton detection to enhance the sensitivity of solid-state NMR experiments with very low-γ nuclei by one to two orders of magnitude. Coherence transfer between $^{1}$H and low-γ nuclei was performed with low-power double quantum (DQ) or zero quantum (ZQ) cross-polarization (CP) or dipolar refocused insensitive nuclei enhanced by polarization transfer (D-RINEPT). Comparison of the absolute sensitivity of CP NMR experiments performed with proton detection with 1.3 mm rotors and direction detection with 4 mm rotors shows that proton detection with a 1.3 mm rotor provides a significant boost in absolute sensitivity, while requiring approximately 1/40$^{th}$ of the material required to fill a 4 mm rotor. Fast MAS and proton detection were applied to obtain $^{89}$Y and $^{103}$Rh solid-state NMR spectra of organometallic complexes. These results demonstrate that proton detection and fast MAS represents a general approach to enable and accelerate solid-state NMR experiments with very low-γ nuclei.

## Introduction

Solid-state NMR spectroscopy is a powerful tool for the study of inorganic materials because it can potentially be applied to nearly all of the elements in the periodic table.[1-3] However, many elements have unfavorable properties for NMR spectroscopy such as low natural abundance, large quadrupole moments (for quadrupolar nuclei with spin $I > ½$) and low gyromagnetic ratios ($\gamma$ and Larmor frequency below that of $^{15}N$). For example, the transition metals silver, tungsten, yttrium and rhodium all possess highly abundant NMR-active isotopes with very low-$\gamma$ (Table S1).[4]

Unfortunately, nuclei with a low-$\gamma$ are often very difficult to observe and manipulate in NMR experiments because $\gamma$ determines the Larmor frequency ($\nu_0 = \gamma B_0$), the radiofrequency (RF) field ($\nu_1 = \gamma B_1$), the equilibrium nuclear magnetization and the magnitude of the induced NMR signal (NMR sensitivity $\propto \gamma^{3/2}$).[5] Furthermore, NMR experiments with low-$\gamma$ nuclei are generally impeded by additional factors such as long longitudinal relaxation times ($T_1$), acoustic ringing, poor coherence transfer efficiency, etc. The sensitivity of solid-state NMR experiments with low-$\gamma$ nuclei has been improved by using cross polarization (CP)[6] to transfer the polarization from high-$\gamma$ nuclei such as $^{19}F$ or $^{1}H$ to the low-$\gamma$ nucleus. For example, Merwin and Sebald applied CP to enhance sensitivity and obtain direct detection $^{109}Ag$, $^{89}Y$ and $^{183}W$ CP magic angle spinning (CPMAS) solid-state NMR spectra.[7-9] However, CP experiments with low-$\gamma$ nuclei often require extremely long contact times in excess of 30 ms that lead to very high probe duty cycles.[9] Subsequently, Levitt and co-workers demonstrated that the dipolar recoupling sequence PRESTO may be used to transfer polarization from $^{19}F$ to $^{109}Ag$ in $AgSbF_6$.[10] The advantage of PRESTO is that dipolar recoupling is only applied on the $^{1}H$ or $^{19}F$

channel greatly reducing the probe duty cycle. However, the sensitivity of CP or PRESTO experiments with low-γ nuclei are often poor because the low-γ nucleus is directly detected.

Proton detection can dramatically improve the sensitivity of NMR experiments with low-γ nuclei. Compared to an NMR spectrum obtained with excitation of the proton spins followed by CP (or PRESTO) and direct detection of the low-γ nucleus, an NMR spectrum obtained with initial excitation and detection of proton spins potentially provides a maximum gain in sensitivity (ξ) of ca. $\xi \approx (\gamma_{1H}/\gamma_X)^{3/2} \times (W_X/W_{1H})^{1/2}$, where $W$ is the full width at half maximum.[5, 11] For example, for the low-γ nuclei $^{89}$Y and $^{103}$Rh proton detection can potentially provide a gain in sensitivity on the order of 92 to 176, respectively (considering only γ). However, efficient proton detection in solid-state NMR requires narrowing of the $^{1}$H NMR signals (reduction of $W_{1H}$), which is most often achieved by using fast MAS frequencies ($\nu_{rot}$) exceeding ca. 25 kHz.[11] For low-γ nuclei such as $^{15}$N it was shown that a sensitivity gain from proton detection (ξ) on the order of 3 was obtained with $\nu_{rot}$ = 28 kHz.[11-12] Fast MAS and proton detection are now routinely applied to indirectly detect common spin-1/2 nuclei such as $^{13}$C, $^{15}$N and $^{29}$Si and the low-γ spin 1 quadrupolar $^{14}$N nucleus.[11-19] Notably, Carnevale *et al*. have recently demonstrated that CP-based pulse sequences can be used to indirectly detect $^{14}$N solid-state NMR spectra with efficiency comparable to heteronuclear multiple quantum coherence spectroscopy (HMQC).[20] We have recently shown that high sensitivity gains can be obtained by employing proton detection to record wideline solid-state NMR spectra of heavy spin-1/2 nuclei and half-integer quadrupolar nuclei.[21-22] We have also recently applied fast MAS and proton detection to observe $^{109}$Ag sites in silver-based ionic liquids for gas chromatography; however, the gains in sensitivity from proton detection were not measured..[23]

Here we demonstrate that fast MAS and proton detection can routinely provide sensitivity enhancements of one to two orders of magnitude for solid-state NMR experiments with very low-γ spin-1/2 nuclei such as $^{89}$Y, $^{103}$Rh, $^{109}$Ag and $^{183}$W. Absolute sensitivity comparisons of solid-state NMR experiments with 4 mm and 1.3 mm rotors demonstrate that proton detection with small diameter rotors provides a significant net gain in absolute sensitivity. Coherence transfer between $^{1}$H and low-γ nuclei was performed with low-power double quantum (DQ) or zero quantum (ZQ) cross-polarization (CP) or dipolar refocused insensitive nuclei enhanced by polarization transfer (D-RINEPT). The limitations and advantages of these different methods are demonstrated experimentally and with numerical simulations. Proton detection and fast MAS are then applied to obtain 2D HETCOR solid-state NMR spectra of yttrium and rhodium organometallic complexes.

**Experimental**

All fast MAS experiments were performed on a double resonance 1.3 mm HX probe, with a Bruker Avance III HD spectrometer and a 9.4 T ($\nu_0(^1H)$ = 400 MHz) wide-bore NMR magnet. Shunt capacitors were inserted in parallel with the primary variable tuning capacitor of X-channel of the probe to tune to the required very low Larmor frequencies. The capacitor for tuning the 1.3 mm HX probe to $^{109}$Ag/$^{183}$W was provided courtesy of Mr. Albert Donkoh (Bruker Biospin Inc., Billerica, MA). Additional capacitors were purchased from NMR Service Inc. and the shunt capacitor inserts for the probe were made by soldering copper strips onto the capacitors (Figure S1, Table S2). Experiments with large diameter rotors were performed on a 4 mm triple resonance HXY probe configured in double resonance mode. The probe was tuned to $^{183}$W/$^{109}$Ag by adding capacitor inserts in parallel to the X-channel variable tuning capacitor.

Fast MAS solid-state NMR experiments using the 1.3 mm HX probe were performed at a 50 kHz MAS frequency. The $^1$H $T_1$ was measured with saturation recovery for all the samples and optimum recycle delays of 1.3 × $T_1$ were used for all experiments shown in the main text except where noted otherwise. The pulse calibrations were performed directly on each sample using a $\pi/2$ – spin-lock pulse sequence (Figure S2) by determining the second order rotary resonance recoupling ($R^3$) condition ($2 \times \nu_{rot}$)[24] and the HORROR ($0.5 \times \nu_{rot}$)[25] conditions. The calibrated 100 kHz RF power was utilized for all $^1$H $\pi/2$ and $\pi$ pulses. In the 2D HETCOR NMR experiments, unwanted background $^1$H magnetization was removed by saturation blocks consisting of a $\pi/2$ pulse followed by a 300 – 500 μs spin-lock pulse at the HORROR condition and a 10 – 25 ms dephasing delay (Figure S3).[26] The saturation blocks were generally repeated 10 to 20 times. The HORROR condition was also applied for heteronuclear decoupling during the $t_1$-evolution periods in the 2D HETCOR experiments and during acquisition in the direct detected 1D experiments.[25] Proton detected CP-HETCOR NMR spectra were acquired with the standard pulse sequence[11] that uses forwards CP, z-storage, $^1$H saturation and back-CP steps (Figure S3A). Alternatively, D-RINEPT pulse sequences[22, 27] were also used for proton detection, where the forwards and backwards CP steps were replaced with D-RINEPT blocks (Figure S3B).

The double-quantum and zero-quantum CP conditions ($\nu_1(^1\text{H}) \pm \nu_1(\text{X}) = n \times \nu_{rot}$) were optimized directly on the samples of interest by observing the intensity of the 1D $^1$H detected CP signal as a function of $^1$H spin-lock RF fields with a fixed RF field for the X spin-lock pulse. Unless specifically indicated, all CP experiments were performed under $n = 1$ conditions, the precise CP conditions are listed in Table S3. All CP experiments employed ramped $^1$H spin-lock pulses with a 95%-100% amplitude ramp on the forward ($^1$H→X) CP blocks and a 100%-95%

amplitude ramp on the backward (X→$^{1}$H) CP blocks.[28] Figure S4 shows a comparison between experimental and SIMPSON simulations of the $^{1}$H-$^{109}$Ag CPMAS optimizations. The lengths of the X $\pi/2$ pulses were directly optimized on each sample using the $^{1}$H detected CP experiment (Figure S3A). An example of this optimization is provided in Figure S4D and the optimized pulse lengths and experimental conditions for all the samples are listed in Table S3. Other parameters used to acquire and process the spectra are listed in Table S4. In the D-RINEPT experiments symmetry based $SR4_1^2$ recoupling[29] was applied on the $^{1}$H channel at the optimized 100 kHz RF fields ($2 \times \nu_{rot}$). The duration of each recoupling block ($m \times \tau_r$ in Figure S3, where $\tau_r$ corresponds to one rotor period) was directly optimized on each sample to give maximum signal. Proton $T_{1\rho}$ and $T_2$' during $SR4_1^2$ recoupling were measured using the pulse sequences shown in Figure S2 and fit in MATLAB to the equation $S(\tau) = A \times \exp(-\tau / T)$ where $\tau$ was the duration of the spin-lock pulses or recoupling pulse sequence, $T$ is the $T_{1\rho}$ or $T_2$' time constants (Table S5) and $A$ is the fit signal intensity at $\tau = 0$. The proton detected $^{1}$H-$^{103}$Rh D-RINEPT $J$-resolved experiment was performed using the pulse sequence shown in Figure S3B. The simultaneous application of $\pi$ pulses on the $^{1}$H and $^{103}$Rh channels in the $J$-resolved block causes signal dephasing due to evolution of $^{103}$Rh-$^{1}$H scalar couplings. The experiment was performed in an interleaved manner where for each $\tau_J$ value, a control experiment was also performed with the application of only the $^{103}$Rh $\pi$-pulse (Figure S5).[30-31] A normalized $J$-dephasing curve free from transverse relaxation was then constructed by dividing each $J$-dephased data point by the corresponding control data point. The normalized $J$-dephasing curve was fit to a simple cosine function, $S(\tau_J) = \cos(\pi \times J \times \tau_J)$, to determine $^{1}J(^{103}\text{Rh},^{1}\text{H})$. Fitting was performed using the curve fitting tool in MATLAB 8.6.0 (R2015b).

Solid-state NMR experiments using 4 mm rotors were performed at a MAS rate of 8 kHz. The $^{1}$H pulses were calibrated by recording a nutation curves and determining the 2π-pulse. The RF on the X-channel was initially determined by acquiring $^{109}$Ag spin echo NMR spectra using a solution of 9 M $AgNO_3$ in $D_2O$. After optimization of CP conditions a more accurate pulse calibration was performed directly using a CP – $\pi/2_{flip\text{-}back}$ – $\pi/2_{read}$ pulse sequence (Table S6). $^{1}$H→$^{183}$W and $^{1}$H→$^{109}$Ag CPMAS experiments used $^{183}$W/$^{109}$Ag spin-lock pulses with ca. 12 kHz RF field (ca. 80 – 95 W of input power) on the $^{183}$W/$^{109}$Ag channel and the matching $^{1}$H spin-lock pulse RF field was optimized for maximum signal (Table S6). Optimum CPMAS signal was obtained with $^{1}$H spin-lock RF fields of 20 kHz and 27 kHz for $^{183}$W and $^{109}$Ag NMR experiments, respectively (Table S7) with a 95%-100% amplitude ramp. These CP conditions correspond to zero-quantum CP conditions ($\nu_{1,X} + n*\nu_{rot} = \nu_{1,1H}$) with $n$ = 1 for $^{183}$W and $n$ = 2 for $^{109}$Ag. The $n$ = 2 CP condition likely gave more signal for $^{109}$Ag CPMAS experiments on silver methanesulfonate because the $^{1}$H $T_{1\rho}$ increases with higher $^{1}$H spin-lock RF fields. High quality direct detected CP spectra for sensitivity comparisons were obtained using a CP spin echo pulse sequence with a total spin echo 4 rotor cycles in duration to eliminate acoustic ringing. All other acquisition and processing parameters were the same as the corresponding fast MAS direct detected experiments (Table S4).

$^{1}$H NMR chemical shifts were referenced to neat tetramethylsilane using adamantane ($\delta_{iso}$($^{1}$H) = 1.82 ppm) as a secondary chemical shift standard. $^{89}$Y, $^{103}$Rh, $^{109}$Ag and $^{183}$W chemical shifts were indirectly referenced using the previously published relative NMR frequencies.[4] The average of four signal-to-noise ratio (SNR) measurements were considered for calculating the sensitivities of all NMR spectra. All NMR spectra were processed in Bruker Topspin 3.5 pl7.

DFT calculations were performed on compound **1** with plane-wave pseudopotentials and periodic boundary conditions using CASTEP.[32] The heavy-atom positions were fixed from the X-ray crystal structure and the hydrogen atom positions were optimized prior to performing NMR parameter calculations. All calculations used the Perdew-Burke-Ernzerhof (PBE) generalized gradient approximation (PBE-GGA) functional[33] with the Tkatchenko-Scheffler (TS) dispersion (DFT-D) correction scheme[34] and ultra-soft pseudopotentials generated *on-the-fly*.[35] $P_1$ symmetry was imposed on the unit cell prior to performing NMR calculations. Magnetic shielding, electric field gradient and *J*-coupling tensors were calculated using the GIPAW method[36] implemented in CASTEP under the Zero-Order Relativistic Approximation (ZORA).[37-38] Optimizations were converged to a kinetic energy cut-off of 630 eV for the plane-wave basis set. The integrals were calculated over a Brillouin zone with a minimum *k*-point spacing of 0.07 $Å^{-1}$. SIMPSON *v*4.1.1[39-41] was used to perform all numerical simulations.

## Results and Discussion

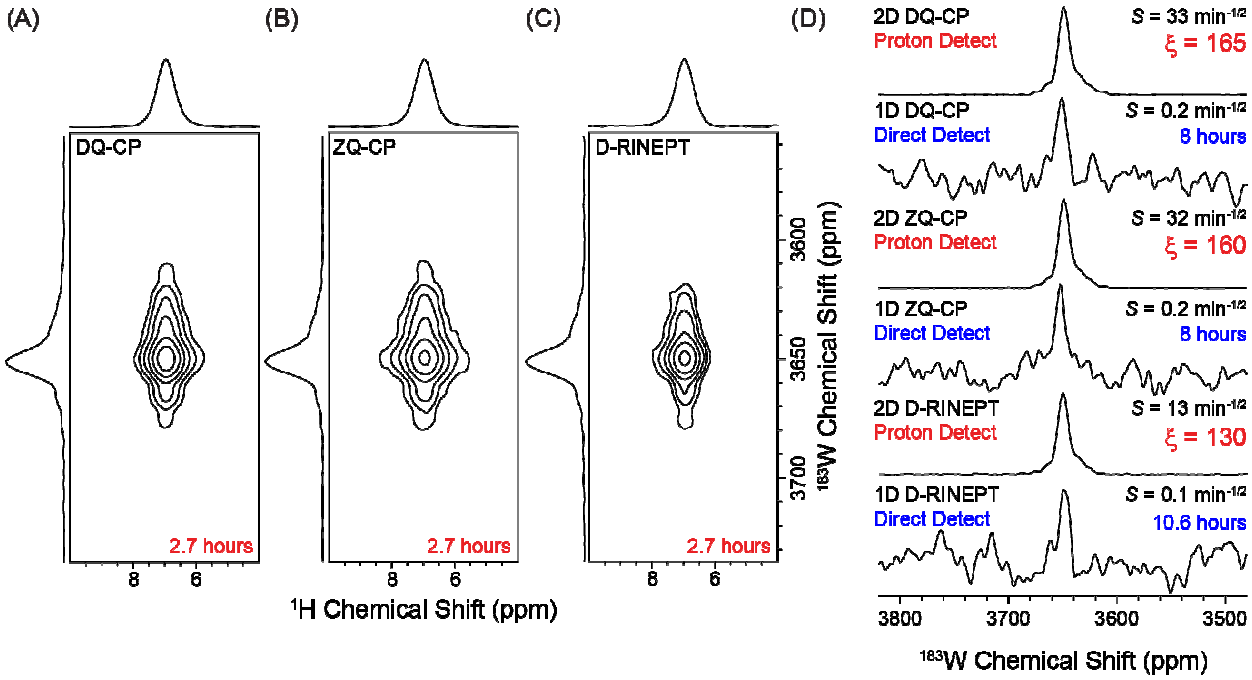


**Figure 1.** $^{183}$W solid-state NMR spectra of ammonium tetrathiotungstate ($(NH_4)_2WS_4$). 2D $^1$H{$^{183}$W} HETCOR NMR spectra obtained with (A) DQ-CP, (B) ZQ-CP and (C) D-RINEPT for coherence transfers. (D) Comparison of $^{183}$W solid-state NMR spectra obtained with direct detection of $^{183}$W using DQ-CP, ZQ-CP and D-RINEPT methods and the positive projections from the corresponding 2D HETCOR NMR spectra. The absolute sensitivity (*S*) and the gain in sensitivity from proton detection (ξ) are indicated next to the NMR spectra. The total experiment times are indicated for the 2D HETCOR and the 1D direct detected $^{183}$W NMR spectra.

First, $^{183}$W NMR is used to demonstrate the potential of proton detection and fast MAS ($\nu_{rot}$ = 50 kHz in all cases) to accelerate solid-state NMR experiments with low-γ nuclei. $^{183}$W has a natural isotopic abundance (NA) of 14.3% and $\nu_0(^{183}W)$ = 16.7 MHz at a magnetic field of 9.4 T ($\nu_0(^1H)$ = 400 MHz). Ammonium tetrathiotungstate ($(NH_4)_2WS_4$) was chosen as a setup compound for $^{183}$W solid-state NMR because its chemical shift and CP characteristics have been previously reported.[8] The total experiment times, number of scans, signal-to-noise ratio (SNR) and sensitivity ($S$ = SNR x $t^{-1/2}$, where $t$ is the total experiment time) for all direct detection and proton detection experiments are compared in Table 1. The recycle delays in both proton

detected and direct detected experiments are determined by the proton $T_1$ ($T_1$ = 14.4 s for $(NH_4)_2WS_4$). In all experiments the recycle delay was set to $1.3\times T_1$ to maximize sensitivity (the recycle delay was 18.7 s for $(NH_4)_2WS_4$, Table 1).

Prior to discussing the NMR results, we briefly describe the CP conditions accessible with fast MAS. Under MAS, the RF fields used for CP obey the modified Hartmann-Hahn match conditions.[42-46] With fast MAS it is possible to use low-power double-quantum (DQ-CP) and zero-quantum (ZQ-CP) conditions.[46-49] For DQ-CP, $\nu_1(^1H) + \nu_1(X) = n \times \nu_{rot}$, while for ZQ-CP, $\nu_1(^1H) - \nu_1(X) = n \times \nu_{rot}$ (with $n$ = 1 for both conditions). For all of the $^{183}W$ CP NMR experiments, $\nu_1(^{183}W) \approx 15$ kHz and $\nu_{rot}$ = 50 kHz, therefore, $\nu_1(^1H) \approx 65$ kHz for ZQ-CP and $\nu_1(^1H) \approx 35$ kHz for DQ-CP. Numerical simulations using SIMPSON[39-41] on a test $^1H$-$^{109}Ag$ two-spin system confirm that both conditions operate at similar efficiencies in the absence of relaxation (Figure S4). With the 1.3 mm double resonance probe used here, the $^1H$ CP spin-lock pulse power required input powers of only 0.4 W (35 kHz) and 1.3 W (65 kHz) for DQ-CP and ZQ-CP, respectively. Only 8.0 W of input power was required to obtain a $\nu_1(^{183}W)$ of 15 kHz. Therefore, both DQ-CP and ZQ-CP conditions can be accessed with low input powers and low probe duty. The low probe duty enables long CP contact times in excess of 20 ms that are required for efficient CP, without risking damage to the probe or pre-amplifiers. The CP conditions used for all the experiments are provided in the SI (Table S3).

The choice of whether to use DQ-CP or ZQ-CP is dictated by the $^1H$ longitudinal relaxation times in the rotating frame ($T_{1\rho}$). A $^1H$ spin-lock experiment can be used to measure the proton $T_{1\rho}$ at the $^1H$ spin-lock RF fields required for the two CP conditions (Figure S2). Whichever $^1H$ spin-lock RF field gives the longest $T_{1\rho}$ will generally give the best CP efficiency. The $^1H$ $T_{1\rho}$ of $((NH_4)_2WS_4)$ was 200 ms and 275 ms at spin-lock RF fields of 35 kHz and 64

kHz, respectively (Table S3) and accordingly the ZQ-CP condition was slightly more efficient than DQ-CP. The CP contact time was directly optimized on all of the samples. For $(NH_4)_2WS_4$ the CP signal continuously increased as the CP contact time for each step was increased up to 30 ms (Figure S6). However, the CP contact time of the forwards and backwards steps were limited to 30 ms (60 ms total contact time) to avoid damaging the probe or pre-amplifiers.

8 hours of signal averaging (1536 scans) were required to obtain the direct detection $^{1}H \rightarrow ^{183}W$ DQ-CP and ZQ-CP NMR spectra of $(NH_4)_2WS_4$ which gave a SNR of only 3.4 and 4.0, corresponding to a *S* of 0.2 $min^{-1/2}$ for both experiments (Figure 1D). The isotropic chemical shift of the $^{183}W$ resonance is 3648 ppm, in agreement with the previously reported value.[8] On the other hand, the 1D proton detected DQ-CP and ZQ-CP $^{1}H\{^{183}W\}$ NMR spectra gave a SNR of 97 and 92 after only 10 minutes of signal averaging (32 scans), corresponding to a *S* of 31 $min^{-1/2}$ and 29 $min^{-1/2}$ (Table 1, Figure S7). Comparison of the sensitivities of the 1D proton detected and $^{183}W$ detected DQ-CP NMR spectra shows that the gain in sensitivity due to proton detection ($\xi$) is ca. 155 (31 $min^{-1/2}$/0.2 $min^{-1/2}$). The experimentally observed $\xi$ of 155 is greater than the expected gain for $^{183}W$ and $^{1}H$ considering only the $\gamma$ of each nucleus ($\xi \approx (\gamma_{1H}/\gamma_{183W})^{3/2}$ = 118). Note that the $^{1}H$ and $^{183}W$ linewidths (*W*) are comparable, therefore, the $^{1}H$ channel of the probe is likely more efficient than the $^{183}W$ channel of the probe, which typically further favors proton detection.[11] In order to obtain a proton detected $^{183}W$ solid-state NMR spectrum, full 2D $^{1}H\{^{183}W\}$ DQ-CP and ZQ-CP heteronuclear correlation (HETCOR) NMR spectra were obtained (Figure 1A and 1B). The 2D CP HETCOR spectra required a total experiment time of only 2.7 hours each. The $^{183}W$ NMR spectrum obtained from the positive projections of the indirect dimension of the ZQ-CP HETCOR spectrum had a SNR of 414 which correspond to *S* of 33 $min^{-1/2}$ and $\xi$ = 165. This large gain in sensitivity corresponds to a factor 27225 ($\xi^2$)

reduction in total experiment time as compared to the corresponding direct detected $^{1}H \rightarrow ^{183}W$ CPMAS spectra. This result demonstrates the value of the proton detected solid-state NMR experiments for very low-γ nuclei.

**Table 1.** Comparison of sensitivities of proton detected and direct detected $^{183}W$ experiments

| Method | NS | Recycle Delay (s) | Experiment Time (min) | $^{1}H$ Sensitivity SNR | $^{1}H$ Sensitivity SNR•$t^{-1/2}$ ($min^{-1}$) | X Sensitivity SNR | X Sensitivity SNR•$t^{-1/2}$ ($min^{-1/2}$) |
|---|---|---|---|---|---|---|---|
| *Direct* Detection $^{183}W$ NMR Spectra | | | | | | | |
| 1D DQ-CP | 1536 | 18.7 | 478.7 | - | - | 3.4 | 0.2 |
| 1D ZQ-CP | 1536 | 18.7 | 478.7 | - | - | 4.0 | 0.2 |
| 1D D-RINEPT | 2048 | 18.7 | 638.3 | - | - | 3.4 | 0.1 |
| *Proton* Detected $^{183}W$ NMR Spectra | | | | | | | |
| 1D DQ-CP | 32 | 18.7 | 10.0 | 97 | 31 | - | - |
| 1D ZQ-CP | 32 | 18.7 | 10.0 | 92 | 29 | - | - |
| 1D D-RINEPT | 64 | 18.7 | 20.0 | 53 | 12 | - | - |
| 2D DQ-CP | 2×256 | 18.7 | 159.6 | 337 | 27 | 414 | 33 |
| 2D ZQ-CP | 2×256 | 18.7 | 159.6 | 341 | 27 | 409 | 32 |
| 2D D-RINEPT | 2×256 | 18.7 | 159.6 | 134 | 11 | 166 | 13 |
| $^{1}H$ Spin Echo | 4 | 18.1 | 1.2 | 4289 | 3915 | - | - |

The D-RINEPT pulse sequence[22, 27] (Figure S3) was also utilized to record a 1D $^{1}H \rightarrow ^{183}W$ direct detected and $^{1}H\{^{183}W\}$ 2D HETCOR NMR spectra as shown in Figure 1D and 1C. The D-RINEPT pulse sequence places a very low power demand on the probe and pre-amplifiers because the $^{183}W$ channel only requires rotor-synchronized π/2 and π pulses, while low-power symmetry based $SR4_1^2$ recoupling[29] is applied to the $^{1}H$ channel with an RF field of two times the MAS frequency ($\nu_1(^{1}H) = 2 \times \nu_{rot}$) (Figure S3). The sensitivity of the direct detected $^{1}H \rightarrow ^{183}W$ D-RINEPT experiment was 0.1 $min^{-1/2}$ which is about half the sensitivity of the direct detected CP experiments (Figure 1, Table 1), suggesting that the efficiency of the D-RINEPT experiment is about half that of CP. A full 2D HETCOR spectrum was obtained with D-RINEPT in 2.7 hours (Figure 1C, Table 1), yielding a $^{183}W$ sensitivity of 13 $min^{-1/2}$ on the

positive projection of the indirect $^{183}$W dimension. This corresponds to ξ of 130, which is slightly lower than the ξ of ca. 160 obtained with CP. This reduction in ξ is likely due to low intrinsic efficiency of the D-RINEPT polarization transfer process which is limited by the short $T_2$' of the $^1$H spins under $SR4_1^2$ dipolar recoupling (Table S5). In comparison, the $^1$H $T_{1\rho}$ relaxation times that dictate the efficiency of CP are typically at least an order of magnitude longer (Figure S2, Table S5). However, D-RINEPT provides a larger excitation bandwidth than CP because the finite π/2 and π pulses have a much greater bandwidth than the spin-lock pulses. With the typical RF fields we have used (Table S3), the CP excitation bandwidth is about 8 kHz while the D-RINEPT provides a larger excitation bandwidth of 24 kHz (Figure S8). Many low-γ transition metal nuclei display large chemical shift ranges of several thousand ppm. Therefore, 1D proton detected D-RINEPT could be useful to quickly scan across the chemical shift range and locate the signal of the low-γ nucleus, followed by a CP-based experiment to obtain a higher quality 2D NMR spectrum. We note an alternative CP condition would be to use $\nu_1$(X) = 35 kHz and match this to $\nu_1$($^1$H) = 85 kHz. Simulations suggest that this alternative condition offers improved CP excitation bandwidth of ca. 16 kHz (Figure S8).

$^{109}$Ag (NA = 48.2%) and $^{89}$Y (NA = 100%) solid-state NMR experiments were performed on silver methanesulfonate ($Ag(SO_3CH_3)$) and yttrium nitrate hexahydrate ($Y(NO)_3{\bullet}6H_2O$), respectively, to demonstrate the general applicability of proton detection and fast MAS for very low-γ nuclei. Both of these compounds are used as CP setup standards for these nuclei.[7, 9, 50] These results are summarized in Figure 2, Figure S9-S10 and Table S8. We have very recently applied proton detection and fast MAS to obtain $^{109}$Ag solid-state NMR spectra of several silver-based ionic liquids used as stationary phases in gas chromatography.[23]

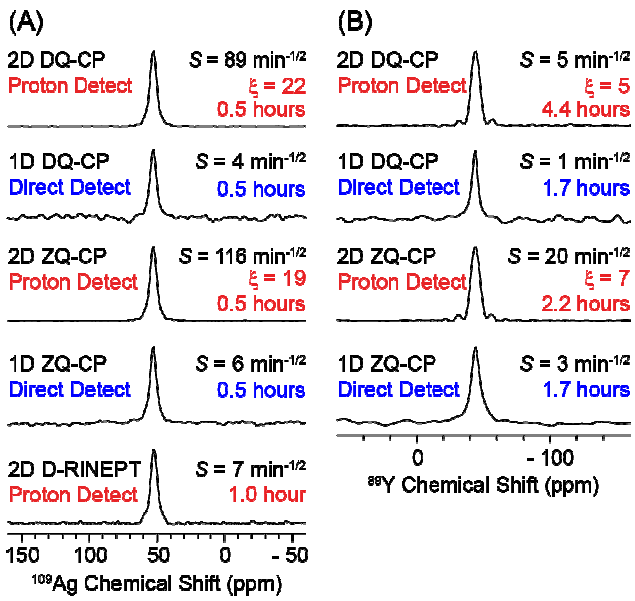


**Figure 2.** Comparison of proton detected and direct detected (A) $^{109}$Ag solid-state NMR spectra of silver methanesulfonate ($AgSO_3CH_3$) and (B) $^{89}$Y solid-state NMR spectra of yttrium nitrate hexahydrate ($Y(NO_3)_3$•$6H_2O$). The CP condition/pulse sequence used for acquisition, sensitivity (*S*), total experiment time and gain in sensitivity from proton detection (ξ) are indicated. The proton detected NMR spectra were obtained from the positive projections of the corresponding 2D HETCOR spectrum.

A ξ of ca. 19 to 22 was obtained for proton detected $^{109}$Ag solid-state NMR experiments on $Ag(SO_3CH_3)$ (Figure 2A). Proton detected D-RINEPT performed significantly worse than the CP experiments, likely due to a short $^1$H $T_2$' during $SR4_1^2$ recoupling (see Table S5). For $^{89}$Y solid-state NMR experiments on $Y(NO)_3$•$6H_2O$ proton detection with CP provided a ξ of 5 to 7. The relatively small ξ values for $Y(NO)_3$•$6H_2O$ likely occur because this sample had a short $^1$H $T_{1\rho}$ (7 ms and 13 ms for DQ-CP and ZQ-CP $^1$H RF fields, respectively). The short $^1$H $T_{1\rho}$ likely occurs due to the dynamics of the coordinated water molecules and/or the very large $^1$H homonuclear dipolar couplings for water. For yttrium, the ZQ-CP condition was preferred because the $^1$H $T_{1\rho}$ was slightly longer at the higher power $^1$H spin-lock RF field used for ZQ-CP. ZQ-CP and DQ-CP required optimal contact times of 16 ms and 10 ms, respectively, which

are much shorter than was required for the other samples and reflect the short $^{1}$H $T_{1\rho}$ (Figure S5). The $^{1}$H $T_2$' during $SR4_1^2$ recoupling was also under 1 ms, which causes a rapid loss of magnetization during the D-RINEPT transfer. Consequently, it was not possible to obtain proton or direct detected $^{1}$H-$^{89}$Y D-RINEPT NMR spectra in a reasonable experiment time. The $^{89}$Y NMR experiments highlight that $^{1}$H $T_{1\rho}$ and $T_2$' during $SR4_1^2$ recoupling are likely to determine the efficiency of proton detection. However, the $^{1}$H $T_{1\rho}$ at different spin-lock RF fields and $T_2$' during $SR4_1^2$ recoupling can usually be rapidly measured before attempting any CP or D-RINEPT experiments and the spectroscopist can decide which CP condition or pulse sequence will likely work the best.

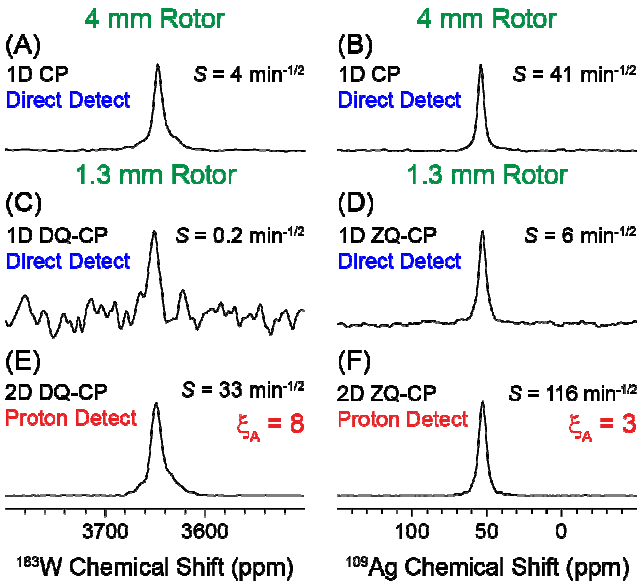


**Figure 3.** Comparison of the absolute sensitivity of proton detection with small diameter rotors and direct detection with large diameter rotors for (left) $^{183}$W NMR experiments on $NH_4WS_4$ and (right) $^{109}$Ag NMR experiments on $Ag(SO_3CH_3)$. Direct detected CPMAS NMR spectra obtained with (A, B) a 4 mm rotor and $\nu_{rot}$ = 8 kHz or (C, D) a 1.3 mm rotor and $\nu_{rot}$ = 50 kHz. (E, F) Proton detected spectra obtained from the positive projections of 2D HETCOR NMR spectra. The gain in absolute sensitivity ($\xi_A$) is indicated. Experiment times, SNR and sensitivities are summarized in Tables S7 and S8.

*Absolute Sensitivity Comparison of Large and Small Diameter Rotors.* The results described above demonstrate that proton detection provides a substantial gain in sensitivity compared to direct detection within the 1.3 mm rotor. However, direct detection CPMAS experiments would most likely be performed with larger diameter rotors because they can potentially provide better absolute sensitivity by virtue of a larger sample volume. Nishiyama has presented an extensive theoretical and experimental investigation of absolute NMR sensitivity for different rotor diameters and shown that absolute sensitivity is approximately proportional to $d^{3/2}$, where $d$ is the rotor diameter.[18] For example, comparing a 1.3 mm and 4 mm rotor, the 1.3 mm rotor should provide ca. 5-fold lower sensitivity because of reduced sample volume.[18] However, proton detection can compensate for this sensitivity reduction, and provide a net gain in sensitivity.

Figure 3 compares the sensitivities of direct detected CPMAS NMR spectra of $NH_4WS_4$ and $Ag(SO_3CH_3)$ obtained with 4 mm diameter rotors (ca. 100 μL sample volume) with the direct detected and proton detected spectra acquired using 1.3 mm diameter rotors (ca. 2.5 μL sample volume). The spectra shown in Figure 3 were acquired with experimental conditions that yielded maximum sensitivities for the different rotors (Tables S6 and S7). Comparing the direct detected CPMAS spectra shows that higher sensitivities of 4 $min^{-1/2}$ and 41 $min^{-1/2}$ are obtained with the 4 mm rotors compared to the lower sensitivities of 0.2 $min^{-1/2}$ and 6 $min^{-1/2}$ obtained with the 1.3 mm rotors for $NH_4WS_4$ and $Ag(SO_3CH_3)$, respectively. Because of the greater amount of material in the 4 mm rotor the direct detection CPMAS experiments with 4 mm rotors provide 7 to 20 times better sensitivity compared to the corresponding experiments with 1.3 mm rotors. However, with proton detected experiments sensitivities of 33 $min^{-1/2}$ and 116 $min^{-1/2}$ were obtained for $^{183}W$ and $^{109}Ag$ using 1.3 mm rotors. Comparison of proton detected 1.3 mm

rotor sensitivity and direct detected 4 mm rotor sensitivity shows that proton detection with a small rotor provides significant gains in absolute sensitivity ($\xi_A$) of factors 8 and 3 for $^{183}$W and $^{109}$Ag NMR spectra, respectively. In summary, proton detection with 1.3 mm rotors provides superior absolute sensitivity for these very low-γ nuclei and requires only 1/40$^{th}$ of the sample as compared to the 4 mm rotor. Addtionally, CP experiments with the 1.3 mm diameter rotor require much lower powers (ca. 8 to 12 W low-γ -spin-lock pulse power) as compared to the 4 mm rotor (ca. 80 – 100 W low-γ spin-lock pulse power). Therefore, with the 1.3 mm rotor, very long CP contact times can be used without risking damage to the probe/spectrometer.

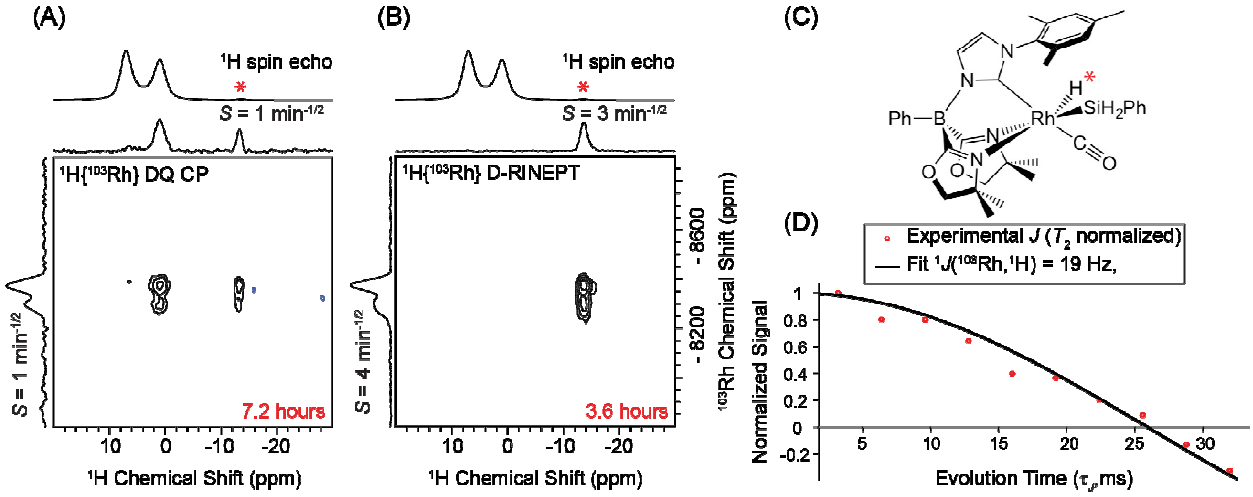


**Figure 4.** $^1$H and $^{103}$Rh solid-state NMR spectra of an organometallic rhodium complex (**1**). Proton detected (A) 2D $^1$H{$^{103}$Rh} DQ-CP spectrum and (B) 2D $^1$H{$^{103}$Rh} D-RINEPT spectrum. (C) Structure of the organometallic rhodium complex. (D) Plot showing the results of a *J*-resolved experiment on **1**. The fit of the *J*-resolved curve yields $^1J(^{103}\text{Rh},^1\text{H})$ = 19 Hz. (Figure S5). The hydride directly attached to rhodium appears at -13.5 ppm in the 1D $^1$H spin echo and has a low relative signal intensity (marked by asterisk).

*Solid-State NMR of Organometallic Compounds.* Proton detection was applied to obtain the $^{103}$Rh solid-state NMR spectrum of a previously reported rhodium complex[51] formed in an $PhSiH_3$ oxidative addition reaction (denoted as compound **1**, Figure 4) which is a precursor to a

catalyst for partial deoxygenation of esters.[52] Although $^{103}$Rh is 100% naturally abundant it has a very low Larmor frequency of only 12.8 MHz at 9.4 T (Table S1). To the best of our knowledge, there has been only one previous report of $^{103}$Rh solid-state NMR spectra,[53] most likely because of the challenges associated with the low-$\gamma$ of $^{103}$Rh.

Figure 4 shows the $^{1}$H spin echo NMR spectrum and proton detected $^{103}$Rh solid-state NMR spectra of **1** that were obtained with 2D DQ-CP and D-RINEPT. The $^{1}$H spin echo spectrum shows a low intensity signal at –13.5 ppm which is assigned to the hydride and much more intense NMR signals from methyl groups and aromatic protons. The $^{103}$Rh NMR spectrum obtained with proton detected D-RINEPT gave a $^{103}$Rh positive projection spectrum that had a SNR of ca. 56 after 3.6 hours of total acquisition. This corresponds to a $^{103}$Rh sensitivity of 3.8 min$^{-1/2}$. The hydride appearing at ca. –13.5 ppm facilitates the polarization transfer between $^{1}$H and $^{103}$Rh due to a relatively strong heteronuclear dipolar coupling of ca. 930 Hz for a 1.6 Å $^{1}$H-$^{103}$Rh distance. The lower sensitivity of the DQ-CP spectrum in comparison to the D-RINEPT spectrum is likely due to the short $^{1}$H $T_{1\rho}$ (Table S5) and because $^{1}$H spin diffusion during the spin-lock pulse distributes $^{1}$H signal intensity across the spectrum. The $^{1}$H spin diffusion is evidenced by the appearance of a cross-peak in the DQ-CP spectrum between the distant methyl groups and the rhodium signal. With D-RINEPT the coherence transfer is more selective because homonuclear $^{1}$H dipolar couplings are suppressed and only a cross-peak between rhodium and the hydride $^{1}$H is observed.

The $^{103}$Rh NMR spectrum of **1** shows two distinct peaks with $^{103}$Rh isotropic chemical shifts of –8300 ppm and –8375 ppm. Initially, we hypothesized that the peak splitting was due to scalar and residual dipolar coupling to $^{14}$N. However, SIMPSON simulations suggest that the residual dipolar couplings to $^{14}$N only results in peak broadening on the order of 2 ppm (Figure

S11). Therefore, we believe that the two distinct $^{103}$Rh isotropic chemical shifts observed are due to different solid forms (polymorphs or solvates). A proton detected $^{1}$H-$^{103}$Rh *J*-resolved experiment was performed using the pulse sequence shown in Figure S3B. This measurement yielded a rhodium-hydrogen one-bond scalar coupling ($^{1}J(^{103}\mathrm{Rh},^{1}\mathrm{H})$) of 19 Hz (Figure S5). The $^{1}J(^{1}\mathrm{H}\text{-}^{103}\mathrm{Rh})$ measured in the solid-state is comparable to the previously reported coupling of 21.3 Hz measured with solution $^{1}$H NMR.[51] Scalar coupling constants predicted with plane-wave DFT implemented in CASTEP[32] are shown in Table S9.

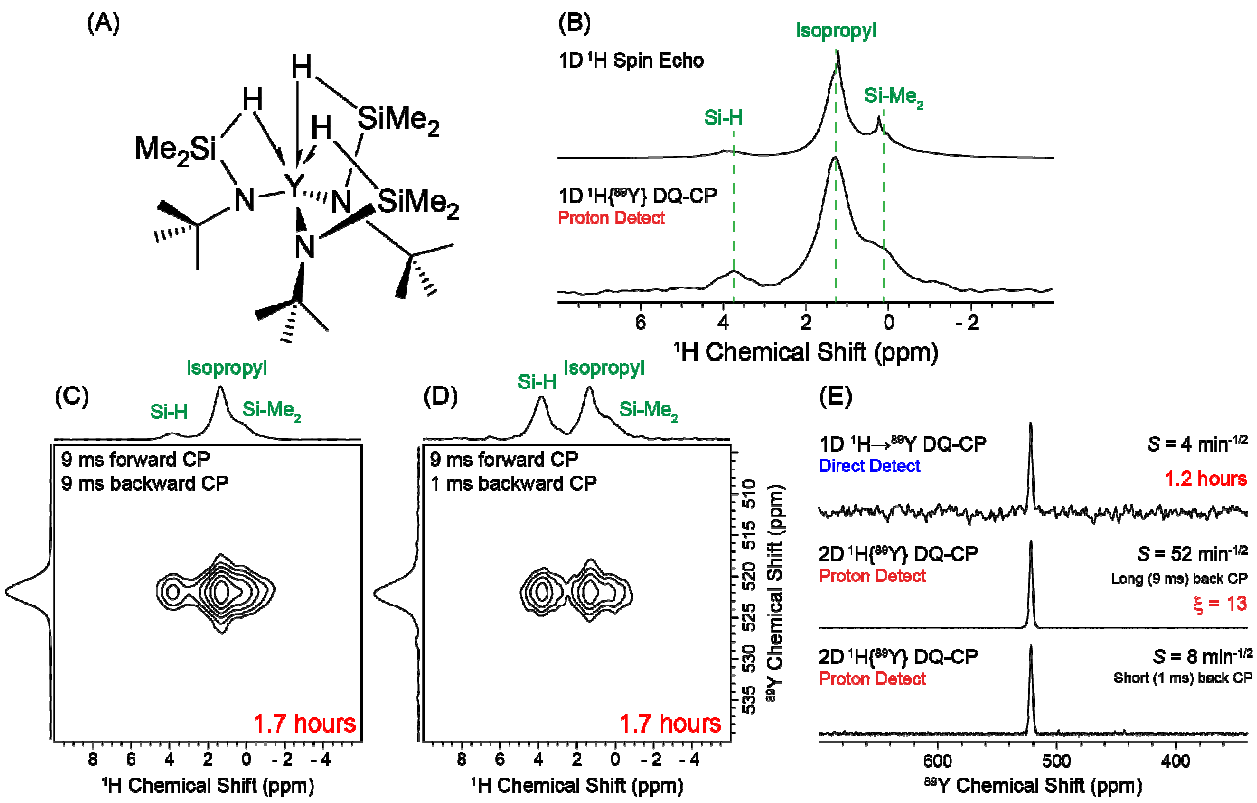


**Figure 5.** $^{1}$H and $^{89}$Y solid-state NMR spectra of compound **2**. (A) Molecular structure of compound **2**. (B) 1D $^{1}$H spin echo spectrum and proton detected 1D $^{1}$H{$^{89}$Y} DQ-CP spectrum. Proton detected 2D $^{1}$H{$^{89}$Y} DQ-CP spectra with (C) 9 ms forward and backward CP contact times and (D) 9 ms forward and 1 ms backward CP contact times. (E) Comparison of direct detected 1D $^{1}$H→$^{89}$Y DQ-CP spectrum with positive projections of $^{89}$Y from the 2D spectra. Sensitivities (*S*) are indicated for the $^{89}$Y spectra shown in (E). The total experiment times are indicated for the direct detected $^{1}$H→$^{89}$Y DQ-CP spectrum and the proton detected 2D $^{1}$H{$^{89}$Y} DQ-CP spectra. All $^{1}$H-$^{89}$Y experiments were performed with a 280 K temperature setting on the variable temperature unit.

Proton detection was also applied to obtain the $^{89}$Y solid-state NMR spectrum of Y{N(SiHMe$_2$)*t*Bu}$_3$ (denoted as compound **2**). **2** has been used for solution-phase grafting of yttrium sites onto silica for heterogeneous hydroamination reactions, and **2** also has potential applications in chemical vapor deposition.[54-55] Notably, high-quality 2D proton detected $^1$H{$^{89}$Y} NMR spectra of **2** were obtained in less than 2 hours (Figure 5). Comparing the sensitivities, a direct detected 1D DQ-CP spectrum had a $S$ of 4 min$^{-1/2}$ whereas the positive projection from the proton detected 2D HETCOR spectrum had a $S$ of 52 min$^{-1/2}$ corresponding to a $\xi$ of 13 (Figures 5C and 5E). As the $^1$H $T_1$ was short for this compound (ca. 0.86 s), the proton detected 2D experiments were acquired with a longer recycle delay of 1.5 s to reduce the probe duty. Note that using a shorter recycle delay would have yielded a higher gain in sensitivity due to proton detection. A second 2D spectrum was obtained with a short $^{89}$Y→$^1$H backward CP contact time to minimize $^1$H spin diffusion during the spin-lock pulse and to enhance the intensity of correlations to more strongly dipolar coupled $^1$H nuclei (Figure 5D). Although a reasonable 2D spectrum was obtainable with a short back CP contact time, the sensitivity of the $^{89}$Y positive projections dropped from 52 min$^{-1/2}$ to 8 min$^{-1/2}$ when the contact time of the back CP step was decreased from 9 ms to 1 ms (Figure 5E). The intense correlations between the Si-H and yttrium peaks are consistent with a relatively short internuclear distance of ca. 2.5 Å that results from secondary bonding interactions between these hydrogen atoms and yttrium.[55]

*Conclusions*

In summary, fast MAS and proton detection were used to accelerate $^{89}$Y, $^{109}$Ag, $^{183}$W and $^{103}$Rh solid-state NMR spectra experiments. In the samples studied here, the gain in sensitivity

provided by proton detection (ξ) was found to be on the order of 5 – 165 which correspond to time-savings of a factor 25 – 27225. The absolute sensitivity of proton detected NMR spectra acquired with 1.3 mm rotors was found to be superior to those obtained with direct detection and 4 mm rotors. For $^{183}$W and $^{109}$Ag NMR spectra, proton detection with a 1.3 mm rotor was found to provide factors 8 and 3 times better sensitivity than direct detection with a 4.0 mm rotor that holds ca. 40 times more sample. Furthermore, the high resolution in the $^{1}$H dimension of 2D HETCOR NMR spectra is easily obtained without the use of homonuclear decoupling sequences. The enormous sensitivity gains and time-savings provided by proton detection should permit the routine characterization of materials containing these elements by solid-state NMR spectroscopy, even in heterogeneous catalysts or inorganic materials where the elements may be very dilute. Dynamic nuclear polarization (DNP) is an alternative approach to enhance the sensitivity of direct detection solid-state NMR experiments with very low-γ nuclei.[55-58] With the development of fast MAS DNP probes[59-60] we anticipate that proton detection and fast MAS could be combined with DNP to obtain further improvements in the sensitivity of solid-state NMR experiments with very low-γ nuclei.

**Acknowledgements**

AV and AJR were supported by the U.S. Department of Energy (DOE), Office of Science, Basic Energy Sciences, Materials Science and Engineering Division. KB, AB, and ADS were supported by U.S. Department of Energy (DOE), Office of Science, Basic Energy Sciences, Chemical Sciences, Geosciences, and Biosciences. The Ames Laboratory is operated for the U.S. DOE by Iowa State University under contract # DE-AC02-07CH11358. AJR thanks Iowa State University and the Ames Laboratory (Royalty Account) for additional support. We are grateful to Mr. Albert Donkoh (Bruker Biospin Inc., Billerica, MA) for providing a capacitor for tuning the 1.3 mm probe to $^{109}$Ag/$^{183}$W.

**Supporting Information**

Additional supplementary tables, figures, and NMR experiment details can be found in the supporting information.

## References


1. Mason, J. *Multinuclear NMR*. First ed.; Plenum Press: New York, **1987**.
2. Bryce, D. L.; Bernard, G. M.; Gee, M.; Lumsden, M. D.; Eichele, K.; Wasylishen, R. E. Practical Aspects of Modern Routine Solid-State Multinuclear Magnetic Resonance Spectroscopy: One-Dimensional Experiments. *Can. J. Anal. Sci. Spect.* **2001,** *46* (2), 46-82.
3. Mackenzie, K. J. D.; Smith, M. E. *Multinuclear Solid-State NMR of Inorganic Materials*. First ed.; Pergamon: Oxford, UK, **2002**.
4. Harris, R. K.; Becker, E. D.; De Menezes, S. M. C.; Goodfellow, R.; Granger, P. NMR Nomenclature. Nuclear Spin Properties and Conventions for Chemical Shifts - (IUPAC recommendations 2001). *Pure Appl. Chem.* **2001,** *73* (11), 1795-1818.
5. Ernst, R. R.; Bodenhausen, G.; Wokaun, A. *Principles of Nuclear Magnetic Resonance In One and Two Dimensions*. Second ed.; Oxford University Press: Oxford, **1987**.
6. Pines, A.; Gibby, M. G.; Waugh, J. S. Proton-Enhanced NMR of Dilute Spins in Solids. *J. Chem. Phys.* **1973,** *59* (2), 569-590.
7. Merwin, L. H.; Sebald, A. The First $^{89}$Y CP-MAS Spectra. *J. Magn. Reson.* **1990,** *88* (1), 167-171.
8. Merwin, L. H.; Sebald, A. Cross-Polarisation to Low-Gamma Nuclei: the First $^{183}$W CP/MAS Spectra. *Solid State Nucl. Magn. Reson.* **1992,** *1* (1), 45-47.
9. Merwin, L. H.; Sebald, A. The First Examples of $^{109}$Ag CP-MAS Spectroscopy. *J. Magn. Reson.* **1992,** *97* (3), 628-631.
10. Zhao, X.; Hoffbauer, W.; Gunne, J. S. A. D.; Levitt, M. H. Heteronuclear Polarization Transfer by Symmetry-based Recoupling Sequences in Solid-State NMR. *Solid State Nucl. Magn. Reson.* **2004,** *26* (2), 57-64.
11. Ishii, Y.; Tycko, R. Sensitivity Enhancement in Solid State $^{15}$N NMR by Indirect Detection with High-Speed Magic Angle Spinning. *J. Magn. Reson.* **2000,** *142* (1), 199-204.
12. Schnell, I.; Langer, B.; Sontjens, S. H. M.; van Genderen, M. H. P.; Sijbesma, R. P.; Spiess, H. W. Inverse Detection and Heteronuclear Editing in $^{1}$H-$^{15}$N Correlation and $^{1}$H-$^{1}$H Double-Quantum NMR Spectroscopy in the Solid State under Fast MAS. *J. Magn. Reson.* **2001,** *150* (1), 57-70.
13. Paulson, E. K.; Morcombe, C. R.; Gaponenko, V.; Dancheck, B.; Byrd, R. A.; Zilm, K. W. Sensitive High Resolution Inverse Detection NMR Spectroscopy of Proteins in the Solid State. *J. Am. Chem. Soc.* **2003,** *125* (51), 15831-15836.
14. Reif, B.; Griffin, R. G. $^{1}$H Detected $^{1}$H-$^{15}$N Correlation Spectroscopy in Rotating Solids. *J. Magn. Reson.* **2003,** *160* (1), 78-83.
15. Cavadini, S.; Antonijevic, S.; Lupulescu, A.; Bodenhausen, G. Indirect Detection of Nitrogen-14 in Solids via Protons by Nuclear Magnetic Resonance Spectroscopy. *J. Magn. Reson.* **2006,** *182* (1), 168-172.
16. Wiench, J. W.; Bronnimann, C. E.; Lin, V. S. Y.; Pruski, M. Chemical Shift Correlation NMR Spectroscopy with Indirect Detection in Fast Rotating Solids: Studies of Organically Functionalized Mesoporous Silicas. *J. Am. Chem. Soc.* **2007,** *129* (40), 12076-12077.
17. Zhou, D. H.; Shah, G.; Cormos, M.; Mullen, C.; Sandoz, D.; Rienstra, C. M. Proton-Detected Solid-State NMR Spectroscopy of Fully Protonated Proteins at 40 kHz Magic-Angle Spinning. *J. Am. Chem. Soc.* **2007,** *129* (38), 11791-11801.
18. Nishiyama, Y. Fast Magic-Angle Sample Spinning Solid-State NMR at 60-100 kHz for Natural Abundance Samples. *Solid State Nucl. Magn. Reson.* **2016,** *78*, 24-36.
19. Kobayashi, T.; Nishiyama, Y.; Pruski, M. Heteronuclear Correlation Solid-state NMR Spectroscopy with Indirect Detection under Fast Magic-Angle Spinning. In *Modern Methods in Solid-state NMR: A Practitioner's Guide*, Hodgkinson, P., Ed. The Royal Society of Chemistry: **2018**; pp 1-38.
20. Carnevale, D.; Ji, X.; Bodenhausen, G. Double Cross Polarization for the Indirect Detection of Nitrogen-14 Nuclei in Magic Angle Spinning NMR Spectroscopy. *J. Chem. Phys.* **2017,** *147* (18).

21. Rossini, A. J.; Hanrahan, M. P.; Thuo, M. Rapid Acquisition of Wideline MAS Solid-State NMR Spectra with Fast MAS, Proton Detection, and Dipolar HMQC Pulse Sequences. *Phys. Chem. Chem. Phys.* **2016,** *18* (36), 25284-25295.
22. Venkatesh, A.; Hanrahan, M. P.; Rossini, A. J. Proton Detection of MAS Solid-State NMR Spectra of Half-Integer Quadrupolar Nuclei. *Solid State Nucl. Magn. Reson.* **2017,** *84*, 171-181.
23. Nan, H.; Zhang, C.; Venkatesh, A.; Rossini, A. J.; Anderson, J. L. Argentation Gas Chromatography Revisited: Separation of Light Olefin/Paraffin Mixtures using Silver-based Ionic Liquid Stationary Phases. *J. Chromatogr. A* **2017,** *1523*, 316-320.
24. Oas, T. G.; Griffin, R. G.; Levitt, M. H. Rotary Resonance Recoupling of Dipolar Interactions in Solid-State Nuclear Magnetic-Resonance Spectroscopy. *J. Chem. Phys.* **1988,** *89* (2), 692-695.
25. De Paepe, G.; Elena, B.; Emsley, L. Characterization of Heteronuclear Decoupling through Proton Spin Dynamics in Solid-State Nuclear Magnetic Resonance Spectroscopy. *J. Chem. Phys.* **2004,** *121* (7), 3165-3180.
26. Ishii, Y.; Yesinowski, J. P.; Tycko, R. Sensitivity Enhancement in Solid-State $^{13}$C NMR of Synthetic Polymers and Biopolymers by $^{1}$H NMR Detection with High-Speed Magic Angle Spinning. *J. Am. Chem. Soc.* **2001,** *123* (12), 2921-2922.
27. Trebosc, J.; Hu, B.; Amoureux, J. P.; Gan, Z. Through-Space $R^3$-HETCOR Experiments between Spin-1/2 and Half-Integer Quadrupolar Nuclei in Solid-State NMR. *J. Magn. Reson.* **2007,** *186* (2), 220-227.
28. Metz, G.; Wu, X. L.; Smith, S. O. Ramped-Amplitude Cross-Polarization in Magic-Angle-Spinning NMR. *J. Magn. Reson. Ser. A.* **1994,** *110* (2), 219-227.
29. Brinkmann, A.; Kentgens, A. P. M. Proton-Selective $^{17}$O-$^{1}$H Distance Measurements in Fast Magic Angle Spinning Solid-State NMR Spectroscopy for the Determination of Hydrogen Bond Lengths. *J. Am. Chem. Soc.* **2006,** *128* (46), 14758-14759.
30. Trebosc, J.; Amoureux, J. P.; Delevoye, L.; Wiench, J. W.; Pruski, M. Frequency-Selective Measurement of Heteronuclear Scalar Couplings in Solid-State NMR. *Solid State Sci.* **2004,** *6* (10), 1089-1095.
31. Zhao, L.; Hanrahan, M. P.; Chakravarty, P.; DiPasquale, A. G.; Sirois, L. E.; Nagapudi, K.; Lubach, J. W.; Rossini, A. J. Characterization of Pharmaceutical Cocrystals and Salts by Dynamic Nuclear Polarization-Enhanced Solid-State NMR Spectroscopy. *Cryst. Growth Des.* **2018**.
32. Clark, S. J.; Segall, M. D.; Pickard, C. J.; Hasnip, P. J.; Probert, M. J.; Refson, K.; Payne, M. C. First Principles Methods using CASTEP. *Z. Kristallogr.* **2005,** *220* (5-6), 567-570.
33. Perdew, J. P.; Burke, K.; Ernzerhof, M. Generalized Gradient Approximation Made Simple. *Phys Rev Lett* **1996,** *77* (18), 3865-3868.
34. Tkatchenko, A.; Scheffler, M. Accurate Molecular Van Der Waals Interactions from Ground-State Electron Density and Free-Atom Reference Data. *Phys Rev Lett* **2009,** *102* (7).
35. Yates, J. R.; Pickard, C. J.; Mauri, F. Calculation of NMR Chemical Shifts for Extended Systems using Ultrasoft Pseudopotentials. *Phys. Rev. B* **2007,** *76* (2).
36. Pickard, C. J.; Mauri, F. All-Electron Magnetic Response with Pseudopotentials: NMR Chemical Shifts. *Phys. Rev. B* **2001,** *63* (24).
37. Green, T. F. G.; Yates, J. R. Relativistic Nuclear Ragnetic Resonance J-Coupling with Ultrasoft Pseudopotentials and the Zeroth-Order Regular Approximation. *J. Chem. Phys.* **2014,** *140* (23).
38. Joyce, S. A.; Yates, J. R.; Pickard, C. J.; Mauri, F. A First Principles Theory of Nuclear Magnetic Resonance J-Coupling in Solid-State Systems. *J. Chem. Phys.* **2007,** *127* (20).
39. Bak, M.; Rasmussen, J. T.; Nielsen, N. C. SIMPSON: A General Simulation Program for Solid-State NMR Spectroscopy. *J. Magn. Reson.* **2000,** *147* (2), 296-330.
40. Tosner, Z.; Andersen, R.; Stevenss, B.; Eden, M.; Nielsen, N. C.; Vosegaard, T. Computer-Intensive Simulation of Solid-State NMR Experiments using SIMPSON. *J. Magn. Reson.* **2014,** *246*, 79-93.
41. Tosner, Z.; Vosegaard, T.; Kehlet, C.; Khaneja, N.; Glaser, S. J.; Nielsen, N. C. Optimal Control in NMR Spectroscopy: Numerical Implementation in SIMPSON. *J. Magn. Reson.* **2009,** *197* (2), 120-134.

42. Schaefer, J.; Stejskal, E. O. $^{13}$C Nuclear Magnetic-Resonance of Polymers Spinning at Magic Angle. *J. Am. Chem. Soc.* **1976,** *98* (4), 1031-1032.
43. Stejskal, E. O.; Schaefer, J.; Waugh, J. S. Magic-Angle Spinning and Polarization Transfer in Proton-Enhanced NMR. *J. Magn. Reson.* **1977,** *28* (1), 105-112.
44. Sardashti, M.; Maciel, G. E. Effects of Sample Spinning on Cross Polarization. *J. Magn. Reson.* **1987,** *72* (3), 467-474.
45. Wind, R. A.; Dec, S. F.; Lock, H.; Maciel, G. E. $^{13}$C CP-MAS and High Speed Magic Angle Spinning. *J. Magn. Reson.* **1988,** *79* (1), 136-139.
46. Meier, B. H. Cross Polarization under Fast Magic Angle Spinning - Thermodynamical Considerations. *Chem. Phys. Lett.* **1992,** *188* (3-4), 201-207.
47. Marks, D.; Vega, S. A Theory for Cross-Polarization NMR of Nonspinning and Spinning Samples. *J. Magn. Reson. Ser. A.* **1996,** *118* (2), 157-172.
48. Laage, S.; Marchetti, A.; Sein, J.; Pierattelli, R.; Sass, H. J.; Grzesiek, S.; Lesage, A.; Pintacuda, G.; Emsley, L. Band-Selective $^{1}$H-$^{13}$C Cross-Polarization in Fast Magic Angle Spinning Solid-State NMR Spectroscopy. *J. Am. Chem. Soc.* **2008,** *130* (51), 17216-17217.
49. Laage, S.; Sachleben, J. R.; Steuernagel, S.; Pierattelli, R.; Pintacuda, G.; Emsley, L. Fast Acquisition of Multi-Dimensional Spectra in Solid-State NMR Enabled by Ultra-Fast MAS. *J. Magn. Reson.* **2009,** *196* (2), 133-141.
50. Penner, G. H.; Li, W. L. A Standard for Silver CP/MAS Experiments. *Solid State Nucl. Mag. Reson.* **2003,** *23* (3), 168-173.
51. Xu, S. C.; Manna, K.; Ellern, A.; Sadow, A. D. Mixed N-Heterocyclic Carbene-Bis(oxazolinyl)borato Rhodium and Iridium Complexes in Photochemical and Thermal Oxidative Addition Reactions. *Organometallics* **2014,** *33* (23), 6840-6860.
52. Xu, S. C.; Boschen, J. S.; Biswas, A.; Kobayashi, T.; Pruski, M.; Windus, T. L.; Sadow, A. D. Mild Partial Deoxygenation of Esters Catalyzed by an Oxazolinylborate-Coordinated Rhodium Silylene. *Dalton T.* **2015,** *44* (36), 15897-15904.
53. Phillips, B. L.; Houston, J. R.; Feng, J.; Casey, W. H. Observation of Solid-State $^{103}$Rh NMR by Cross-Polarization. *J. Am. Chem. Soc.* **2006,** *128* (12), 3912-3913.
54. Rees, W. S.; Just, O.; Schumann, H.; Weimann, R. Structural Characterization of a Tris-Agostic Lanthanoid-H-Si Interaction. *Angew. Chem. Int. Edit.* **1996,** *35* (4), 419-422.
55. Eedugurala, N.; Wang, Z. R.; Yan, K. K.; Boteju, K. C.; Chaudhary, U.; Kobayashi, T.; Ellern, A.; Slowing, I. I.; Pruski, M.; Sadow, A. D. Beta-SiH-Containing Tris(silazido) Rare-Earth Complexes as Homogeneous and Grafted Single-Site Catalyst Precursors for Hydroamination. *Organometallics* **2017,** *36* (6), 1142-1153.
56. Blanc, F.; Sperrin, L.; Lee, D.; Dervisoglu, R.; Yamazaki, Y.; Haile, S. M.; De Paepe, G.; Grey, C. P. Dynamic Nuclear Polarization NMR of Low-gamma Nuclei: Structural Insights into Hydrated Yttrium-Doped BaZrO3. *J. Phys. Chem. Lett.* **2014,** *5* (14), 2431-2436.
57. Delley, M. F.; Lapadula, G.; Nunez-Zarur, F.; Comas-Vives, A.; Kalendra, V.; Jeschke, G.; Baabe, D.; Walter, M. D.; Rossini, A. J.; Lesage, A.; Emsley, L.; Maury, O.; Coperet, C. Local Structures and Heterogeneity of Silica-Supported M(III) Sites Evidenced by EPR, IR, NMR, and Luminescence Spectroscopies. *J. Am. Chem. Soc.* **2017,** *139* (26), 8855-8867.
58. Lee, D.; Leroy, C.; Crevant, C.; Bonhomme-Coury, L.; Babonneau, F.; Laurencin, D.; Bonhomme, C.; De Paepe, G. Interfacial $Ca^{2+}$ Environments in Nanocrystalline Apatites Revealed by Dynamic Nuclear Polarization Enhanced $^{43}$Ca NMR Spectroscopy. *Nat. Commun.* **2017,** *8*.
59. Chaudhari, S. R.; Berruyer, P.; Gajan, D.; Reiter, C.; Engelke, F.; Silverio, D. L.; Coperet, C.; Lelli, M.; Lesage, A.; Emsley, L. Dynamic Nuclear Polarization at 40 kHz Magic Angle Spinning. *Phys. Chem. Chem. Phys.* **2016,** *18* (15), 10616-10622.
60. Chaudhari, S. R.; Wisser, D.; Pinon, A. C.; Berruyer, P.; Gajan, D.; Tordo, P.; Ouari, O.; Reiter, C.; Engelke, F.; Coperet, C.; Lelli, M.; Lesage, A.; Emsley, L. Dynamic Nuclear Polarization Efficiency Increased by Very Fast Magic Angle Spinning. *J. Am. Chem. Soc.* **2017,** *139* (31), 10609-10612.

## TOC GRAPHIC